Storey-Based Stability of Unbraced Steel Frames under Piece-Linear Temperature Distributions

Terence Ma[1], Lei Xu[1]

[1]Department of Civil and Environmental Engineering, University of Waterloo, 200 University Avenue West, Waterloo, ON., N2L 3G1, Canada

Corresponding Author:
Lei Xu, University of Waterloo
200 University Avenue West
Waterloo, ON. N2L 3G1
Tel: (519) 888-4567 x36882
Email: lxu@uwaterloo.ca

Abstract

There are many cases where the elastic modulus of a structural member will vary longitudinally, such as when a steel column is heated by fire. In such a case, the fire can compromise the integrity of the structural frame. It is therefore necessary in stability analysis to accurately analyze members with longitudinally varying elastic modulus. A new analytical method is derived to evaluate the stability of an unbraced steel frame containing members that each consist of up to three segments of differing elastic modulus. The method is presented in the form of a lateral stiffness equation, which characterises the loss of stability in a frame when its lateral stiffness diminishes to zero. The proposed method is also demonstrated via a numerical example by analyzing the case of a post-blast explosion fire whereby the insulation along a segment of any member is damaged. A scenario analysis was also conducted to identify the most vulnerable location in a frame, whereby the damage to insulation resulting from a blast causes the greatest reduction to the fire resistance. From a design standpoint, the most vulnerable locations can be identified and further protected to improve safety. The proposed method provides more accurate assessments of frame stability in cases where elastic modulus vary longitudinally in members, and is validated via finite element analysis.

Keywords: fire; stability; steel frame; unbraced; storey-based; segment; stepped; temperature distributions; semi-rigid; insulation damage

1. INTRODUCTION

It is not uncommon for fires to occur in large buildings, especially those containing steel frames. As a result, the effect of fires on structural steel frames has frequently been modeled numerically in the past few decades [1-4]. However, due to the variable and unpredictable nature of fire, assumptions will always be necessary in numerical models. Very often, these assumptions include uniform member temperatures, such as in the cases of [1,5-6]. However, Xu and Zhuang [3] demonstrated that the stability calculations of a steel frame can be significantly affected when a two-stepped temperature distribution is modeled in its columns, rather than assuming uniform temperature. The reason for using two-stepped columns is that room fires exhibit higher temperatures near ceilings and lower temperatures near floors [3]. As such, the assumption of two-stepped members is a progressive step towards realistic modelling of non-linear temperature distributions in columns. Presented in this paper is a new methodology that evaluates the storey-based lateral stability of an unbraced steel frame and extends the use of stepped members towards applications where both columns and beams in a frame contain up to three segments of differing temperatures. The presence of multiple segments of varying temperatures in members of a frame can result from various fire scenarios, such as when fires initiate closer to one side of a compartment, or when insulation is damaged during a post-earthquake or explosion fire. Furthermore, an approach is presented for determining the individual buckling load three-stepped column, which is the upper limit for the applicability of the lateral stiffness equation [7]. The proposed method is demonstrated via numerical example whereby the damage to insulation due to a blast explosion is modelled as a segment along any members of a frame. The heating of the frame in fire until failure under various blast explosion scenarios is modelled to determine the location in the frame whereby the blast results in the highest reduction to its fire resistance.

2. BACKGROUND

The proposed method is in the form of a storey-based stability problem. The concept of storey-based stability was initiated by Yura [8], who noted the fact that lateral instability could only occur with all columns in the frame buckling simultaneously, and that structural frames perform better when considered in whole over its individual members. Subsequently, LeMessurier [9], Lui [10] and Aristizabal-Ochoa [11] have developed matrix methods for the storey stability analysis of steel frames. Xu [12] later derived the lateral stiffness equation for a frame subjected to axial loading with considering P-Δ effects. Recently, Xu and Zhuang [3] extended Xu's method [12] to include members with elevated temperatures under fire, including columns containing two temperature zones along their lengths. However, the method proposed by Xu and Zhuang [3] does not apply for more complicated thermal distributions in the frame members, such as in the case of a large compartment containing a localized fire or travelling fire [4], or when considering the effects of insulation delamination at plastic hinges caused by seismic loading [13-16]. To account for all of these considerations, the proposed method is in the form of a lateral stiffness equation for a storey frame with members containing up to three segments of uniform temperatures. Note that the purpose of this paper is not to detail the modelling process for any specific fire scenario, but to propose a method for assessing the lateral stability assuming that the temperatures in each segment of each member have been determined via other analyses. A variety of analysis approaches are already available to determine the temperatures and deformation of steel members in fire, such as the use of finite element modelling [14] or other numerical procedures such as [5,17-18].

3. PROPOSED MODEL

Consider the 2D storey frame with n bays shown in Fig. 1. All frame members consist of three segments with different temperatures, assumed to be uniform within the segments. For columns, the lower, middle, and upper segments are denoted by the primary subscripts l, m, and u, respectively. For beams, the left, middle, and right segments are denoted by the primary subscripts L, M, and R, respectively. The beams and bays are numbered with primary subscripts from 1 to n, and columns are numbered with secondary subscripts from 1 to n+1.

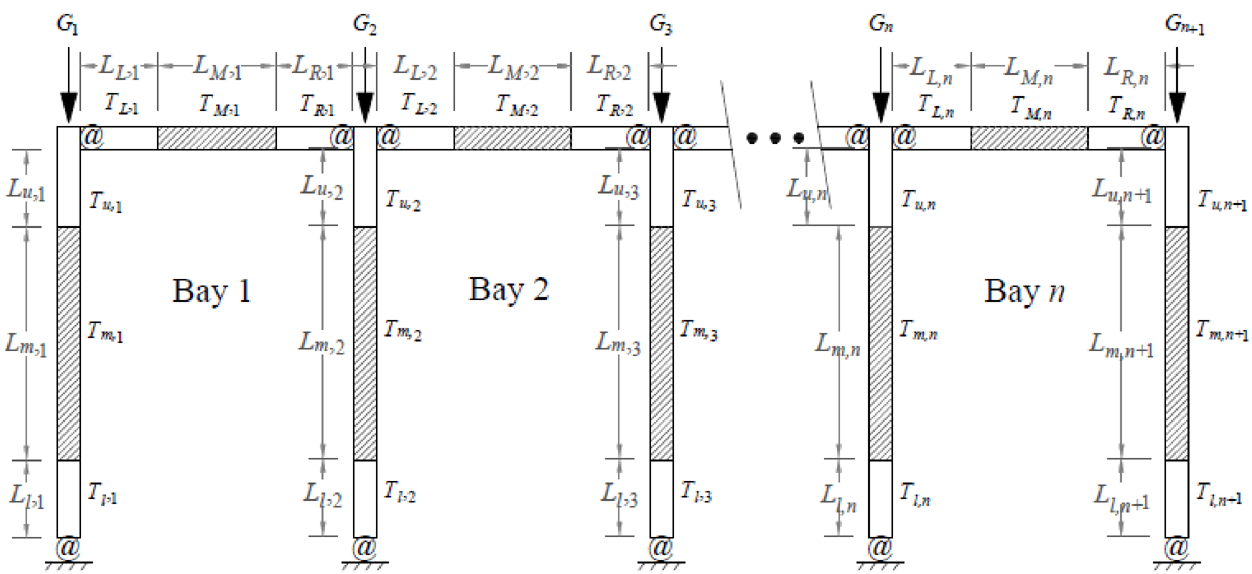

Figure 1 – Schematic of unbraced storey frame with three-segmented members

The temperatures and lengths of each member are denoted in Fig. 1 by the variables T and L, respectively. Let the subscripts i and j correspond to the primary subscript of the columns and beams in the frame, respectively. $I_{c,i}$ and $I_{b,j}$ are the moments of inertia of column i and beam j, respectively. The moment of inertia is assumed to be constant over the entire length of each member. Let $L_{c,i} = L_{u,i} + L_{m,i} + L_{l,i}$ be the height of column i, and $L_{b,j} = L_{L,j} + L_{M,j} + L_{R,j}$ be the length of beam j. The frame is subjected to prescribed gravity loads, G_i. The Eurocode 3 [19] method was adopted to model the degradation of the members due to elevated temperature, and considers the tangent modulus of elasticity as a function of the axial load, *P*, and temperature, *T*, given in Eq. (1).

$$E(P,T)=\mu_T E_0; \quad \mu_T=\frac{1}{E_0}\begin{cases} E_a(T) & , \quad \sigma \le f_p(T) \\ (b/a)(\varepsilon_y(T)-\varepsilon)[a^2-(\varepsilon_y(T)-\varepsilon)^2]^{-0.5} & , f_p(T)<\sigma<f_y(T) \\ 0 & , \quad \sigma \ge f_y(T) \end{cases} \tag{1}$$

Where E_0 is the elastic modulus of the segment at ambient temperature and μ is the degradation factor for the elastic modulus. σ and ε are the stress and strain in the segment, respectively, and *a* and *b* are coefficients defined in Euroocde 3 [19]. E_a, f_p and f_y are the modulus in the linear elastic range, proportional limit and yield stress, respectively, also defined in Eurocode 3 [19] and are functions of the temperature. Note that the proposed methodology can be extended to account for non-fire scenarios, where E_0 can be any reference elastic modulus, and μ can be directly specified based on the relative elastic modulus in each segment.

3.1 End Fixity Factors for Three-Segment Members

All connections in the frame are generalized as semi-rigid connections. The end fixity factor concept established by Monforton and Wu [20] was employed to model the rotational stiffness of these connections. The end fixity factor, *r*, is defined as the ratio between the rotation at the end of the member, *α*, and the combined rotation, ϕ, of the member and the connection due to a unit end-moment, as shown in Fig. 2.

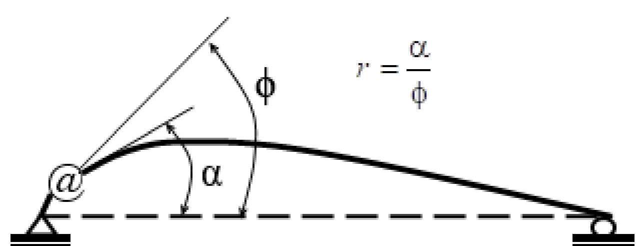

Figure 2 – Definition of End-fixity Factor

Let the upper and lower end fixity factors of column *i* be denoted $r_{u,i}$ and $r_{l,i}$, respectively. Similarly, let the end fixity factors at the corresponding ends of beam *j* be $r_{L,j}$ and $r_{R,j}$, respectively. The end fixity factors for members with three segments of constant elastic modulus are derived in Appendix C and are given in Eqs. (2a) and (2b), respectively, for the columns and beams in the frame.

$$r_{l,i} = \frac{1}{1+\dfrac{3E_0 I_{c,i}}{L_c R_{l,i}\tau_{l,i}}}; \quad r_{u,i} = \frac{1}{1+\dfrac{3E_0 I_{c,i}}{L_c R_{u,i}\tau_{u,i}}} \tag{2a}$$

$$r_{L,j} = \frac{1}{1+\dfrac{3E_0 I_{b,j}}{L_c R_{L,j}\tau_{L,j}}}; \quad r_{R,i} = \frac{1}{1+\dfrac{3E_0 I_{b,j}}{L_c R_{R,j}\tau_{R,j}}} \tag{2b}$$

Where R is the rotational stiffness of the connection at the corresponding end subjected to elevated temperature and τ is an adjustment factor given in Eqs. (4) to account for the different temperatures in the segments. Note that for semi-rigid connections subjected to elevated temperature, R can be adjusted via a reduction factor, k_R, in Eqs. (3) [21].

$$R(T_R) = k_R R_0 \tag{3a}$$

$$k_R = 1 - \frac{m}{R_0} T_R \geq 0 \tag{3b}$$

Where R_0 is the rotational stiffness of the connection at ambient temperature and T_R is the elevated temperature of the connection. For the purpose of simplicity, T_R may be taken as the temperature of the nearest member segment. The value of k_R can be obtained by correlations based on the experimental data in Al-Jabri et al. [22], whereby it is shown for various types of connections that the rotational stiffness parameter in the Ramberg-Osgood [23] rotational stiffness is linearly correlated with temperature. Based on the experimental results, the linear stiffness reduction slope factor, m, ranges between 1×10^4 and 6×10^4 Nm/°C [22]. Note that for idealized connections ($R = 0$ or $R = \infty$, corresponding to $r = 0$ or $r = 1$), the rotational stiffness is unaffected by temperature when using Eq. (3).

The end fixity factors in Eqs. (2) differ from those derived by Monforton and Wu [20] in that they consider members with three segments via a τ factor, which accounts for the differences in temperatures in each segment and is defined in Eqs. (4a) and (4b) for columns and beams, respectively.

$$\begin{aligned}\tau_{l,i} &= \frac{1}{\mu_{l,i}}\left(\frac{L_{l,i}}{L_{c,i}}\right)^3+\frac{1}{\mu_{m,i}}\left(\left(\frac{L_{l,i}+L_{m,i}}{L_{c,i}}\right)^3+\left(\frac{L_{u,i}}{L_{c,i}}\right)^3\right)+\frac{1}{\mu_{u,i}}\left(1-\left(\frac{L_{l,i}+L_{m,i}}{L_{c,i}}\right)^3\right)\\ \tau_{u,i} &= \frac{1}{\mu_{u,i}}\left(\frac{L_{u,i}}{L_{c,i}}\right)^3+\frac{1}{\mu_{m,i}}\left(\left(\frac{L_{u,i}+L_{m,i}}{L_{c,i}}\right)^3+\left(\frac{L_{l,i}}{L_{c,i}}\right)^3\right)+\frac{1}{\mu_{l,i}}\left(1-\left(\frac{L_{u,i}+L_{m,i}}{L_{c,i}}\right)^3\right)\end{aligned} \tag{4a}$$

$$\begin{aligned}\tau_{L,j} &= \frac{1}{\mu_{L,j}}\left(\frac{L_{L,j}}{L_{b,j}}\right)^3+\frac{1}{\mu_{M,i}}\left(\left(\frac{L_{L,j}+L_{M,j}}{L_{b,j}}\right)^3+\left(\frac{L_{R,j}}{L_{b,j}}\right)^3\right)+\frac{1}{\mu_{R,j}}\left(1-\left(\frac{L_{L,j}+L_{M,j}}{L_{b,j}}\right)^3\right)\\ \tau_{R,j} &= \frac{1}{\mu_{R,j}}\left(\frac{L_{R,j}}{L_{b,j}}\right)^3+\frac{1}{\mu_{M,i}}\left(\left(\frac{L_{R,j}+L_{M,j}}{L_{b,j}}\right)^3+\left(\frac{L_{L,j}}{L_{b,j}}\right)^3\right)+\frac{1}{\mu_{L,j}}\left(1-\left(\frac{L_{R,j}+L_{M,j}}{L_{b,j}}\right)^3\right)\end{aligned} \tag{4b}$$

Where μ is the degradation factor accounting for the effect of elevated temperatures on the elastic modulus in the corresponding segment of the member, obtained from Eq. (1). Note that Eqs. (4) extend the case of two-segmented members derived by Xu and Zhuang [3] to include three-segmented members. Therefore, the value of the end fixity factor varies based on the temperature of the segments of the members, as well as the axial load if the segment is in the non-linear elastic range. Note that R = 0 for an idealized pinned connection, and $R = \infty$ for a fixed connection. Similarly, r = 0 for a pinned connection, and r = 1 for a fixed connection. Where multiple beams are connected to the end of column, R is given as the sum of contributions from the beams in Eq. (5).

$$R_{u,i}=\sum_{j_u=1}^{m_u} R_{i,j_u}\,;\quad R_{l,i}=\sum_{j_l=1}^{m_l} R_{i,j_l} \tag{5}$$

Where $R_{u,i}$ and $R_{l,i}$ are the rotational stiffness of the upper and lower end connections, respectively. m_u and m_l are the number of beams connected to the upper and lower ends of column i, respectively. The rotational resistance provided by beam j to column i at the corresponding end, $R_{i,j}$, can be calculated using Eq. (6), with the corresponding derivation shown in Appendix D.

$$R_{i,j} = \frac{6E_0 I_{b,j} r_N}{L_{b,j}} \left[\frac{2\tau_F \mu_L \mu_M \mu_R (1-r_F) + 2\lambda_{NN} r_F + \lambda_{NF} r_F v_{NF}}{4\lambda_A + r_N \lambda_B + r_F \lambda_C - r_N r_F \lambda_D} \right] \tag{6}$$

In which the subscript N refers to the near end of beam j connected to column i, and the subscript F refers to the far end of beam j connected to column i. These subscripts are to be replaced by the subscripts L and R as necessary. The values of μ_N, μ_M, and μ_F for the corresponding segments are obtained from Eq. (1), and v_{NF} is the ratio between the near end and far end connection rotations and corresponds to the buckling shape which needs to be assumed in advance in order to simplify the problem for analytical solutions [24]. It was demonstrated by Xu & Liu [24] that assuming $v_{NF} = 1$ gives accurate estimations of results and corresponds to the asymmetric buckling mode. The coefficients λ_A, λ_B, λ_C, and λ_D are given in Eqs. (7a) through (7d) and are defined such at $\lambda_A = \lambda_D = 1$ and $\lambda_B = \lambda_C = 0$ in the case of a single segment beam with uniform ambient temperature ($\mu_N = \mu_M = \mu_F = 1$). The coefficients λ_{NN} and λ_{NF} depend on the temperatures and lengths of each segment of the member, given in Eqs. (7e) and (7f).

$$\lambda_A = \mu_L \mu_M \mu_R \tau_N \tau_F \tag{7a}$$

$$\lambda_B = 4\tau_F \left(\kappa_N - \tau_N \mu_N \mu_M \mu_F \right) \tag{7b}$$

$$\lambda_C = 4\tau_N \left(\kappa_F - \tau_F \mu_N \mu_M \mu_F \right) \tag{7c}$$

$$\begin{aligned} \lambda_D = 4\left[\tau_F \kappa_N + \tau_N \kappa_F - \tau_N \tau_F \mu_N \mu_M \mu_F\right] - 3L_{b,j}^4 \Big(& L_N^4 \mu_M \mu_F / \mu_N + L_M^4 \mu_N \mu_F / \mu_M + L_F^4 \mu_N \mu_M / \mu_F + \ldots \\ & 4L_N L_M^3 \mu_F + 4L_N L_F^3 \mu_M + 4L_M L_N^3 \mu_F + 4L_M L_F^3 \mu_N + 4L_F L_N^3 \mu_M + 4L_F L_M^3 \mu_N + \ldots \\ & 6L_N^2 L_M^2 \mu_F + 6L_N^2 L_F^2 \mu_M + 6L_M^2 L_F^2 \mu_N + 12L_N^2 L_M L_F \mu_M + 12L_N L_M^2 L_F \mu_M + 12L_N L_M L_F^2 \mu_M \Big) \end{aligned} \tag{7d}$$

$$\lambda_{NN} = \frac{1}{{L_{b,j}}^3}\Big(L_N^3\mu_M\mu_F + L_M^3\mu_N\mu_F + L_F^3\mu_N\mu_M + 3L_N L_M^2\mu_N\mu_F + 3L_N L_F^2\mu_N\mu_M + 3L_M L_N^2\mu_N\mu_F + \ldots$$
$$3L_F L_M^2\mu_N\mu_F + 3L_F L_N^2\mu_F\mu_M + 3L_M L_F^2\mu_M\mu_N + 6L_N L_M L_F\mu_N\mu_M\Big) \tag{7e}$$

$$\lambda_{NF} = \frac{1}{{L_{b,j}}^3}\Big(L_N^3\mu_M\mu_F + L_M^3\mu_N\mu_F + L_F^3\mu_N\mu_M + 3L_N L_M^2\mu_N\mu_F + 3L_N L_F^2\mu_N\mu_M + 3L_M L_N^2\mu_M\mu_F + \ldots$$
$$3L_F L_M^2\mu_N\mu_F + 3L_F L_N^2\mu_F\mu_M + 3L_M L_F^2\mu_N\mu_M + 6L_N L_M L_F\mu_N\mu_F\Big) \tag{7f}$$

Where the coefficients κ_N and κ_F also depend on the temperatures and lengths of each segment of the member and affect the coefficients λ_B, λ_C and λ_D, given in Eqs. (8).

$$\begin{aligned}\kappa_N = \frac{1}{L_{b,j}^4}\Big[&\left(L_N^4\mu_M\mu_F + L_M^4\mu_N\mu_F + L_F^4\mu_N\mu_M\right) + \ldots\\
&3\left(L_N L_M^3\mu_M\mu_F + L_N L_F^3\mu_M\mu_F + L_M L_F^3\mu_N\mu_F\right) + \ldots\\
&4\left(L_M L_N^3\mu_M\mu_F + L_F L_N^3\mu_M\mu_F + L_F L_M^3\mu_N\mu_F\right) + \ldots\\
&\left(L_N L_M^3\mu_N\mu_F + L_N L_F^3\mu_N\mu_M + L_M L_F^3\mu_N\mu_M\right) + \ldots\\
&6\left(L_N^2 L_M^2\mu_M\mu_F + L_N^2 L_F^2\mu_M\mu_F + L_M^2 L_F^2\mu_N\mu_F\right) + \ldots\\
&9\left(L_N L_M^2 L_F\mu_M\mu_F + L_N L_M L_F^2\mu_M\mu_F\right) + \ldots\\
&12\left(L_N^2 L_M L_F\mu_M\mu_F\right) + \ldots\\
&3\left(L_N L_M^2 L_F\mu_N\mu_F + L_N L_M L_F^2\mu_N\mu_F\right)\Big]\end{aligned} \tag{8a}$$

$$\begin{aligned}\kappa_F = \frac{1}{L_{b,j}^4}\Big[&\left(L_N^4\mu_M\mu_F + L_M^4\mu_N\mu_F + L_F^4\mu_N\mu_M\right) + \ldots\\
&3\left(L_M L_N^3\mu_N\mu_F + L_F L_N^3\mu_N\mu_M + L_F L_M^3\mu_N\mu_M\right) + \ldots\\
&4\left(L_N L_M^3\mu_N\mu_F + L_N L_F^3\mu_N\mu_M + L_M L_F^3\mu_N\mu_M\right) + \ldots\\
&\left(L_M L_N^3\mu_M\mu_F + L_F L_N^3\mu_M\mu_F + L_F L_M^3\mu_N\mu_F\right) + \ldots\\
&6\left(L_N^2 L_M^2\mu_N\mu_F + L_N^2 L_F^2\mu_N\mu_F + L_M^2 L_F^2\mu_N\mu_M\right) + \ldots\\
&9\left(L_N L_M^2 L_F\mu_N\mu_M + L_F L_M L_N^2\mu_M\mu_N\right) + \ldots\\
&12\left(L_F^2 L_M L_N\mu_M\mu_N\right) + \ldots\\
&3\left(L_N L_M^2 L_F\mu_N\mu_F + L_F L_M L_N^2\mu_N\mu_F\right)\Big]\end{aligned} \tag{8b}$$

Note that for single segment beams under uniform ambient temperature conditions ($\mu_N = \mu_M = \mu_F = 1$), Eq. (6) converges to the equation for $R_{i,j}$ derived by Monforton and Wu [20]. Where no other members contribute to the rotational rigidity of the end connection of a member, the end fixity factor at the corresponding end may be calculated using Eqs. (3). Expressing this in terms of the end fixity factor at ambient temperature gives Eq. (9) below.

$$r = \frac{r_0 k_R \tau}{1 - r_0(1 - k_R \tau)} \quad (9)$$

Where r is the end fixity factor at the condition-specified end, τ is the corresponding factor in Eqs. (4), and r_0 is the end fixity factor of the corresponding end under ambient temperature conditions. Note that in the cases of pinned connections (r_0 = 0) and fixed connections (r_0 = 1) at ambient temperatures, the resulting end fixity factors at elevated temperatures remain unchanged ($r = r_0$).

3.2 Thermal Restraints

The total axial load of column i experiencing elevated temperatures can be expressed as $P_i = G_i + H_i$, with G_i being the applied gravity load and H_i being the additional axial load induced by restraint against thermal strains. H_i can be taken as zero where there are no physical restraints against thermal strains, or calculated using the procedure in Appendix A for restrained columns.

3.3 Storey-based Lateral Stiffness

In the proposed method, the storey-based lateral stiffness of the frame in Fig. 1 is calculated to evaluate the frame's stability. The lateral stiffness of the frame is its ability to resist lateral deformation under given loading conditions, and is defined as the lateral force required to cause a unit lateral displacement of the storey. The frame becomes unstable when the lateral stiffness of the storey reaches zero [3,12].

In order to evaluate the lateral stiffness of an unbraced frame with three-segmented members, the lateral stiffness of a single three-segmented column illustrated in Fig. 3 must first be derived. For purposes of clarity, the subscript i is removed from Fig. 3 and subsequent equations referring to the variables and properties of this individual column. In order to account for P-Δ effects, the axial load P is also applied to the column.

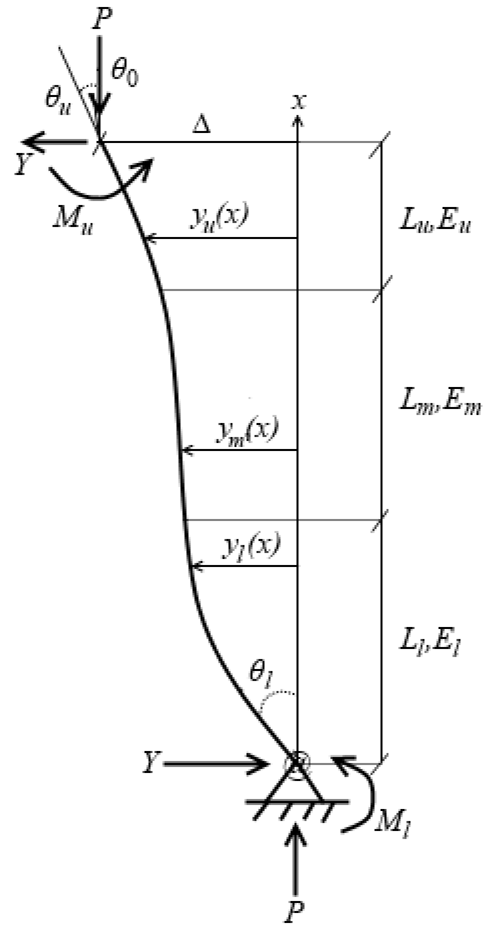

Figure 3 – Single Three-Segment Column subjected to Second Order Effects

A lateral load, Y, is assumed to act at each end of the column. The transverse deflection coordinates $y_l(x)$, $y_m(x)$, and $y_u(x)$ apply to the corresponding segments of the member. The rotational springs at each end of the column produce end moments M_u and M_l as per Eqs. (10).

$$M_u = R_u \theta_u \tag{10a}$$

$$M_l = R_l \theta_l \tag{10b}$$

Where the rotational stiffnesses of the upper and lower connections, R_u and R_l, respectively, can be obtained from Eqs. (3). Based on external equilibrium, Eq. (11) must be satisfied.

$$M_u + M_l = YL_c + P\Delta \tag{11}$$

Based on internal equilibrium via the method of sections, the internal bending moments in the three segments of the column are given in Eqs. (12).

$$E_l I_c \frac{d^2 y_l}{dx^2} = M_l - P\big(y_l(x)\big) - Yx; \quad 0 \le x \le L_l \tag{12a}$$

$$E_l I_c \frac{d^2 y_m}{dx^2} = M_l - P\big(y_m(x)\big) - Yx; \quad L_l \le x \le L_l + L_m \tag{12b}$$

$$E_l I_c \frac{d^2 y_u}{dx^2} = M_l - P\big(y_u(x)\big) - Yx; \quad L_l + L_m \le x \le L_c \tag{12c}$$

The system of differential equations in Eqs. (12) can be solved by applying the eight boundary and compatibility conditions in Eqs. (13), in addition to the external moment equation in Eq. (10).

$$y_l(0) = 0 \tag{13a}$$
$$y_u(L_c) = \Delta \tag{13b}$$
$$y'_l(0) = \theta_l \tag{13c}$$
$$y'_u(L_c) = \theta_u \tag{13d}$$
$$y_l(L_l) = y_m(L_l) \tag{13e}$$
$$y_m(L_l + L_m) = y_u(L_l + L_m) \tag{13f}$$
$$y'_l(L_l) = y'_m(L_l) \tag{13g}$$
$$y'_m(L_l + L_m) = y'_u(L_l + L_m) \tag{13h}$$

Eqs. (13a) through (13d) are boundary conditions at the ends of the column, whereas Eqs. (13e) through (13h) are compatibility conditions that define deformation continuity between each segment of the column. Based on the solution to the system of differential equations in Eqs. (12), the lateral stiffness of the column is equal to Y/Δ, which is expressed in Eqs. (14).

$$\frac{Y}{\Delta} = \frac{\phi^2 E_0 I_c}{L_c^{\,3}} \left(\frac{1}{\psi - 1} \right) \tag{14a}$$

$$\psi = \frac{9 r_u r_l a_5 - 3\phi^2 \left[r_l (1 - r_u) \tau_u + r_u (1 - r_l) \tau_l \right] a_1}{\phi^4 \tau_l \tau_u (1 - r_l)(1 - r_u) a_1 + 9 r_u r_l a_2 - 3\phi^2 \left[r_l (1 - r_u) \tau_u a_3 + r_u (1 - r_l) \tau_l a_4 \right]} \tag{14b}$$

Where the coefficients a_1 through a_5 are given in Eqs. (15).

$$a_1 = \phi_m^2 S_l S_m S_u - \phi_l \phi_m C_l C_m S_u - \phi_m \phi_u S_l C_m C_u - \phi_l \phi_u C_l S_m C_u \tag{15a}$$
$$a_2 = \phi_l^2 \phi_m \phi_u S_l C_m C_u + \phi_l \phi_m^2 \phi_u C_l S_m C_u + \phi_l \phi_m \phi_u^2 C_l C_m S_u - \phi_l^2 \phi_u^2 S_l S_m S_u \tag{15b}$$
$$a_3 = \phi_l^2 \phi_m S_l C_m S_u + \phi_l \phi_m^2 C_l S_m S_u + \phi_l^2 \phi_u S_l S_m C_u - \phi_l \phi_m \phi_u C_l C_m C_u \tag{15c}$$
$$a_4 = \phi_l \phi_u^2 C_l S_m S_u + \phi_m \phi_u^2 S_l C_m S_u + \phi_m^2 \phi_u S_l S_m C_u - \phi_l \phi_m \phi_u C_l C_m C_u \tag{15d}$$
$$a_5 = a_3 + a_4 + 2\phi_l \phi_m \phi_u \tag{15e}$$

in which the modified loading coefficients ϕ_l, ϕ_m and ϕ_u are related to the axial load factor of the column, ϕ, and modified by the degradation factor μ of the corresponding segment due to elevated temperature. S_l, S_m, S_u, C_l, C_m and C_u are all trigonometric functions of the corresponding modified load coefficients associated with each segment of the member. These functions are given in Eqs. (16).

$$\phi = \sqrt{\frac{P}{E_0 I_c}} L_c; \quad \phi_l = \frac{\phi}{\sqrt{\mu_l}}; \quad \phi_m = \frac{\phi}{\sqrt{\mu_m}}; \quad \phi_u = \frac{\phi}{\sqrt{\mu_u}} \tag{16a}$$

$$S_l = \sin\left(\frac{\phi_l L_l}{L_c}\right); \quad S_m = \sin\left(\frac{\phi_m L_m}{L_c}\right); \quad S_u = \sin\left(\frac{\phi_u L_u}{L_c}\right) \tag{16b}$$

$$C_l = \cos\left(\frac{\phi_l L_l}{L_c}\right); \quad C_m = \cos\left(\frac{\phi_m L_m}{L_c}\right); \quad C_u = \cos\left(\frac{\phi_u L_u}{L_c}\right) \tag{16c}$$

Assuming that all of the columns of the storey experience the same deflection, the lateral stiffness of a storey in the frame is the sum of the contributions of the individual columns, given in Eq. (17).

$$\Sigma S = \sum_{i=1}^{n+1} \frac{Y_i}{\Delta} = \sum_{i=1}^{n+1} \left[\frac{\phi_i^{\,2} E_0 I_{c,i}}{L_{c,i}^{\,3}} \left(\frac{1}{\psi_i - 1} \right) \right] \tag{17}$$

This assumption is valid where rigid floor systems are provided to render the beams inextensible. Eq. (17) is applicable as long as P_i is positive and does not exceed the critical load of the individual column, $P_{u,i}$, at which yielding of the section or rotational buckling occurs, shown in Eq. (18).

$$0 \le P_i \le P_{u,i} = \min\{P_{b,i}, P_{y,i}\} \tag{18}$$

Where $P_{y,i}$ is the yielding load of the column equal to the product of the section area and the lowest yield stress in the column, and $P_{b,i}$ is the rotational buckling load determined via Appendix B.

Note that the proposed method applies to one-storey frames. However, it can be extended for use in multi-storey frames either via the storey decomposition method proposed by Liu and Xu [25], whereby a multi-storey frame can be decomposed into individual stories for analysis using the storey-based stability approach. The equivalent rotational stiffness of the column connections can be computed at each storey level, and instability is defined to occur when the product sum of the lateral stiffness in each storey diminishes to zero.

3.4 Modelling of Nonlinear Temperature Distribution

The proposed model using three-segment members can be applied towards different structural engineering applications. Most generally, if non-linear temperature distributions occur in the members, such temperature distributions can be represented using three segments in the proposed method, each with their own average temperatures. Non-linear temperature distributions may result from localized fires, such as when a fire is located in a corner of a room, causing heating at ends of beams. Also, since warm air rises, vertical gradients of temperatures are commonly observed in room fires [3]. Finally, yielding can occur near connections during seismic loading, causing localized loss of fire protection [14-16] and resulting in higher temperatures in the cross sections located in these areas during a post-earthquake fire. In the proposed method, the lateral stiffness of the frame can be calculated if the temperatures of every segment in each member are directly specified. This can be accomplished using any thermal analysis methods, such as the incremental time step method proposed by Pettersson et al. [17], or from finite element analysis. For example, Arablouei and Kodur [14] simulated the effects of localized insulation damage on temperatures in members segments by determining the relative temperatures between insulated and exposed steel obtained from finite element analysis. Relationships between the temperatures of different segments within the frame can therefore be predicted with respect to the fire or reference temperature. In other words, the temperature of a given segment may be taken as a function of either a reference temperature or the duration of fire.

3.5 Computational Procedure

A summary of the procedure that can be followed to analyze the storey-based stability of frames with three-segmented members subjected to fire conditions using the proposed method is provided below.

1. Specify the lengths of the segments in each member (L_l, L_m, L_u, L_L, L_M, L_R). Determine other member properties (I_c, I_b) and specify $v_{NF} = 1$ as necessary.
2. Input the temperatures, T_k, of each segment in each member
3. Input the specified gravity loads, G_i and calculate the thermal restraint forces, H_i, where applicable according to the procedure in Appendix A.
4. Calculate the resulting degradation factors and elastic modulus (μ and E) using the Eurocode 3 [19] method in Eq. (1). Alternatively, E_0 and μ can be specified manually.
5. Calculate the end fixity factors for all ends of all members (r_u, r_l, r_N, r_F) using Eqs. (3). Note that for member ends not dependent on the rotational resistance of other members, r must be adjusted due to elevated temperature according to Eq. (9).
6. Ensure that the values of P_i do not exceed $P_{u,i}$ in Eq. (18). If $P_{u,i}$ is exceeded then the column has failed locally via rotational buckling or yielding.
7. Calculate lateral stiffness contribution, S_i, for each column. The lateral stiffness, ΣS, is the summation of the lateral stiffness contribution from all columns in the storey frame in Eq. (17). If $\Sigma S > 0$ then the frame is stable. Instability analysis can also be performed by increasing either the applied gravity loads or temperatures of the members until instability occurs ($\Sigma S = 0$).

4. NUMERICAL EXAMPLE

A numerical example is provided to demonstrate the use of the proposed method towards a frame with three-segmented members in post-explosion fire scenarios. Explosions in buildings can cause local damages to insulation on members, and the lengths of the regions of damage can be modelled as segments of the members [14]. Moreover, explosions can ignite nearby fuel and cause room fires. Consider the two-bay frame shown in Fig. 4, where the sensitivity of the frame lateral stiffness to the location of insulation damage due to explosion blasts is analyzed.

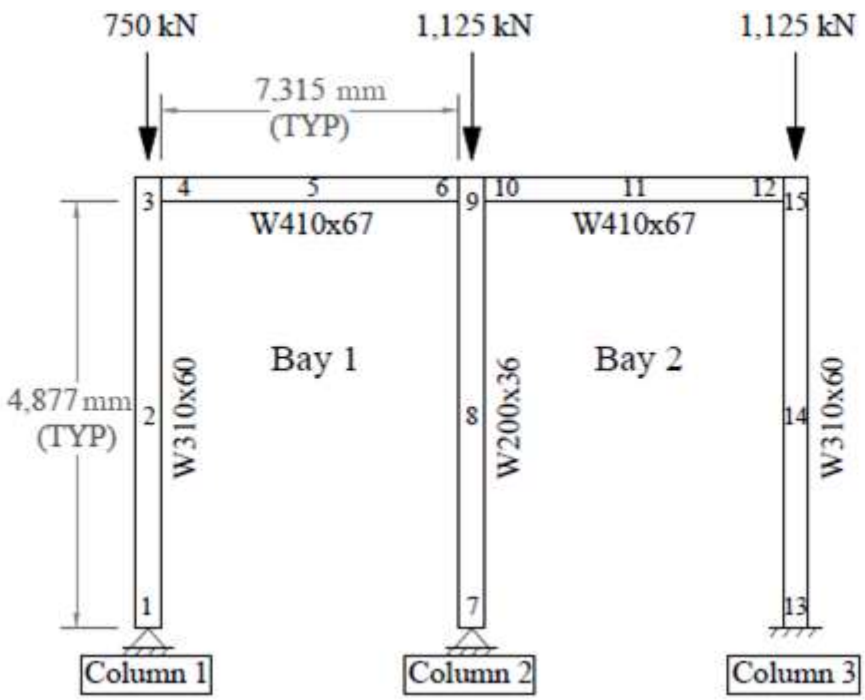

Figure 4 – Example two-bay unbraced storey frame subjected to post-explosion fire

In each scenario, a blast is assumed to cause local delamination to a 1.0 m long segment at either an end or the middle of a member, followed by an ASTM E119 [26] fire, assumed to occur uniformly throughout the entire frame. The member subjected to insulation damage at an end or in the middle can conveniently be modelled as a two- or three-segment member, respectively. Note that single- and two-segment members are modelled as three-segment members with identical properties in adjacent segments. The blast locations are numbered in Fig. 4 for each scenario (1 to 15). The scenarios are also compared to the case of a completely undamaged frame. The original thickness of insulation required to provide a nominal fire resistance of R_N = 120 minutes based on the prescriptive approach in Eq. (19) is applied on each member [27].

$$t_p = \frac{25.4 R_N}{1.03W/D + 42} \tag{19}$$

Where t_p is the thickness of the protective insulation (mm) required to provide the desired fire resistance rating, R (min), for a steel member with unit weight W (kg/m) and heated perimeter D (m). The density, thermal conductivity and heat capacity of insulation are assumed to be 400 kg/m^3, 0.12 W/mK and 1,500 J/kgK, respectively. The section properties are tabulated in Table 1.

Table 1 – Member section properties in two-bay frame example

Property	I	A	D	W	t_p
W200x36	34.1×10^6 mm^4	4,570 mm^2	1.05 m	36 kg/m	39.4 mm
W310x60	129×10^6 mm^4	7,610 mm^2	1.40 m	60 kg/m	35.4 mm
W410x67	245×10^6 mm^4	8,580 mm^2	1.52 m	67 kg/m	34.9 mm

The time-temperature relationships for the segments in each member subjected to the ASTM fire were computed using a 2D heat transfer finite element model in ABAQUS. The gas temperature is assumed to be uniform throughout the frame. Within the 1.0 m delamination length in each scenario, the insulation on one flange of the section is assumed to be removed. The density, thermal conductivity and heat capacity of steel are assumed to be 7,850 kg/m^3, 40 W/mK and 600 J/kgK, respectively. A convective heat transfer coefficient of h = 25 W/m^{2}K and emissivity of 0.9 was assumed for all exposed surfaces. Quadratic heat transfer elements were used in the section meshes. As the blast damage can occur on any one of segment of the members in the frame, all of the sections in Table 1 are illustrated in Fig. 5 as protected with either damaged insulation (DI) and undamaged insulation (UI).

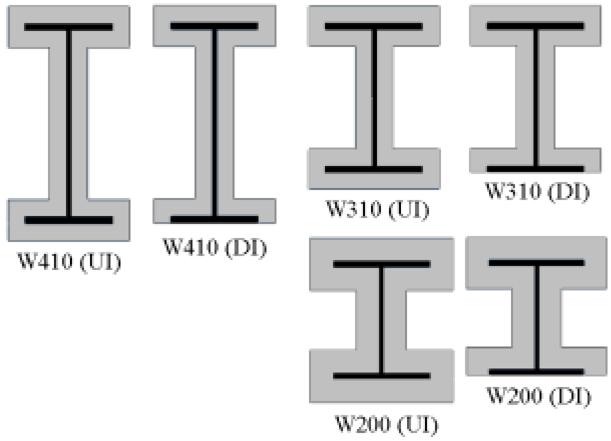

Figure 5 – Cross-sections of segments with damaged insulation (DI) and undamaged insulation (UI)

The cross-sectional temperatures in the member segments under the these cases are plotted versus the duration and gas temperature of the ASTM E119 [26] fire in Fig. 6.

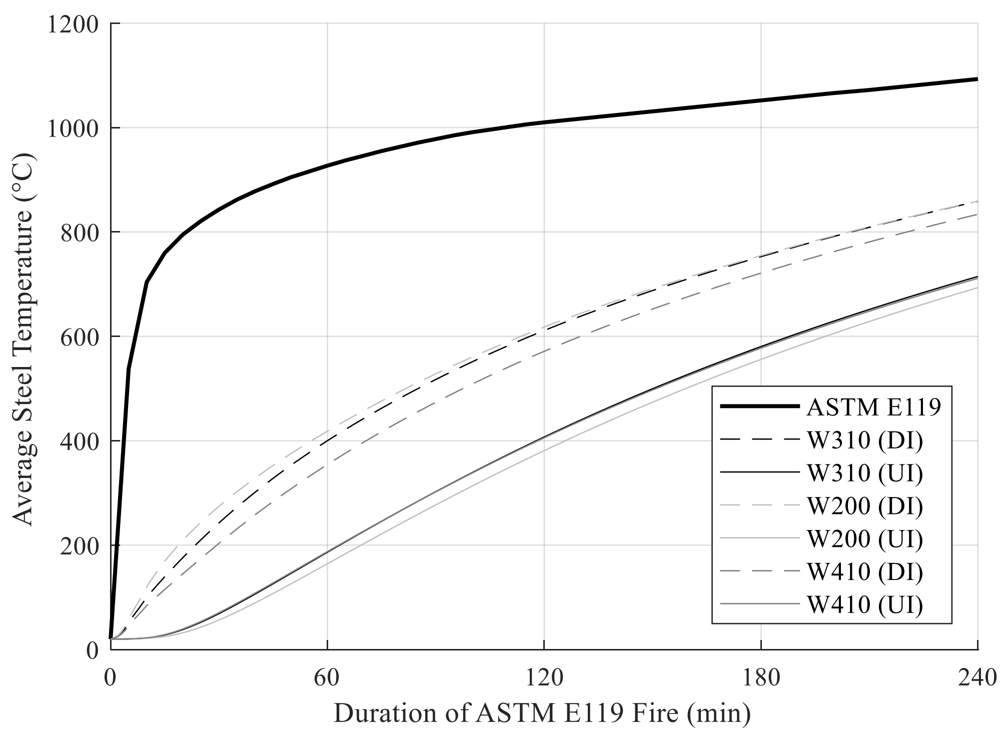

Figure 6 – Time-temperature results from finite element analysis of segment cross-sections

From Fig. (6), it is observed that when any section is subjected to damaged insulation its temperature is increased by up to 255°C over the course of the fire event compared to when it is not damaged. The frame in Fig. 4 is subjected to the prescribed gravity loads shown, which are constant in the analysis. However, the columns are thermally restrained, and the additional axial forces in columns due to thermal expansion will be calculated according to Appendix A. As such, the internal axial forces, P_i, in the columns increase as the temperatures increase. Column 3 is rigidly connected to the ground ($r_{l,3}$ = 1) while the other columns are pinned to the ground ($r_{l,1}$ = $r_{l,2}$ = 0). The ambient modulus of elasticity is E_0 = 200 GPa. All beam-to-column connections are assumed to be semi-rigid end plate connections, with $r_{N,0} = r_{F,0}$ = 0.493 for all beams in Eq. (8), which corresponds to ambient rotational stiffnesses of $R_0 = 19.56\times10^6$ Nm. The linear stiffness reduction slope factor is taken as $m = 2.88\times10^4$ Nm/°C. The R_0 and m parameters were selected based on a linear regression analysis of the results of Al-Jabri et al. [22] for Group 2 end plate connections. The coefficient of determination for fitting the experimental data with the selected parameters was R^2 = 0.97. As the duration of fire is increased, the lateral stiffness of the frame subjected to blast damages diminishes. The duration of fire at which lateral instability failure of the frame occurs, along with the maximum value of $P_i/P_{u,i}$ at the time of failure, is listed for each of the scenarios in Table 2, where $P_{u,i}$ is the rotational buckling load that varies with temperature. The failure times corresponding to two analyses are reported in Table 2: (1) with assuming asymmetrical buckling (v_{NF} = 1) as necessary in the proposed method, and (2) with values of v_{NF} calibrated at each beam-to-column connection based on an eigenvalue buckling analysis conducted in ABAQUS.

Table 2 – Failure durations of fire in scenario analysis of frame subjected to post-explosion fires

Scenario	Damaged Location	Failure Time (v_{NF} = 1)	Failure Time (v_{NF} calibrated)	$(P_i/P_{u,i})_{max}$
U	Undamaged frame	138.8 min	136.2 min	$P_2/P_{u,2}$ = 0.90
1	Column 1, lower end	136.7 min	134.9 min	$P_2/P_{u,2}$ = 0.89
2	Column 1, middle	129.9 min	128.8 min	$P_1/P_{u,1}$ = 0.85
3	Column 1, upper end	131.8 min	130.2 min	$P_1/P_{u,1}$ = 0.86
4	Beam 1, left end	134.7 min	132.5 min	$P_2/P_{u,2}$ = 0.87

5	Beam 1, middle	138.8 min	135.9 min	$P_2/P_{u,2} = 0.90$
6	Beam 1, right end	138.4 min	136.3 min	$P_2/P_{u,2} = 0.90$
7	Column 2, lower end	101.4 min	101.0 min	$P_2/P_{u,2} = 0.99$
8	Column 2, middle	107.0 min	104.6 min	$P_2/P_{u,2} = 0.97$
9	Column 2, upper end	109.7 min	109.7 min	$P_2/P_{u,2} = 1.00$*
10	Beam 2, left end	138.1 min	136.5 min	$P_2/P_{u,2} = 0.90$
11	Beam 2, middle	138.8 min	135.8 min	$P_2/P_{u,2} = 0.90$
12	Beam 2, right end	130.6 min	128.6 min	$P_2/P_{u,2} = 0.85$
13	Column 3, lower end	107.6 min	103.7 min	$P_3/P_{u,3} = 0.78$
14	Column 3, middle	121.0 min	120.4 min	$P_3/P_{u,3} = 0.98$
15	Column 3, upper end	120.9 min	120.7 min	$P_3/P_{u,3} = 0.98$

* Denotes a value that is slightly below but rounds to unity

To obtain the calibrated values for each scenario, the frame in Fig. 4 was modelled in ABAQUS by using B23 cubic Euler-Bernoulli (non-shear-deformable) wireframe elements in all members. The semi-rigid connections were also modelled using linear-elastic “Join + Rotation” connector section features, with temperature-dependent values of R. In the eigenvalue buckling analysis, the loads were proportionally assigned. The thermal restraints were considered by applying an additional factor to the gravity loads equal to the proportional increase in axial load experienced by the column due to the thermal restraints as calculated via the procedure in Appendix A. The time of failure corresponding to the calibrated v_{FN} values in Table 2 were obtained via trial and error in changing the elastic modulus of the segments based on Eq. (1) and repeating the eigenvalue buckling analysis in ABAQUS until the critical applied gravity load factor of the frame corresponded exactly to the given applied loads. The calibrated values of v_{NF} were then retrieved from the FEA model based on the rotational displacements from the buckled shape of the frame at the time of failure in ABAQUS. These values were inputted to the proposed method for re-analysis, and the failure times as determined using the proposed method with the calibrated values are presented in the corresponding column of Table 2. The resulting time of failure differed by at most only 0.02 minutes (0.015%) between the proposed method and the FEA model out of all the scenarios. Further to this, the time of failure obtained using the calibrated v_{FN} values in the proposed method were inputted into ABAQUS whereby the resulting critical load factor was calculated. The proportional load factors applied in ABAQUS were 1, 1 and 1.5, corresponding to Columns 1, 2 and 3, respectively. As such, a critical load factor of 750 kN would correspond to zero error between the FEA model and the proposed method. Out of all of the scenarios, the largest error in the critical load factor calculated in ABAQUS was only 0.909 kN, and corresponded to a critical load factor of 749.091 kN. This difference of only 0.12% is negligible and may have resulted from interpolations used by ABAQUS on the temperatures located at nodes between adjacent segments, and/or truncation errors in the input form for the applied loads. Figs. 7 through 10 illustrate the buckled shapes of the frame in Scenarios U, 2, 7 and 13, as obtained from the FEA model, respectively. Scenarios 2, 7 and 13 correspond to the minimum time of failure resulting from blast damage applied to any segment on Columns 1, 2 and 3, respectively.

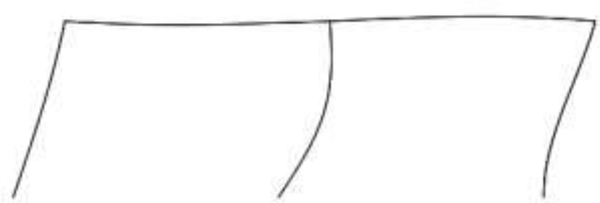

Figure 7 – Buckled shapes of frames in Scenario U (no damage to insulation)

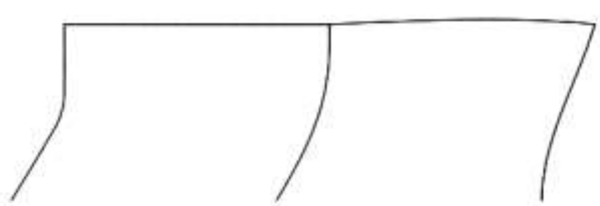

Figure 8 – Buckled shapes of frames in Scenario 2 (worst case delamination in Column 1)

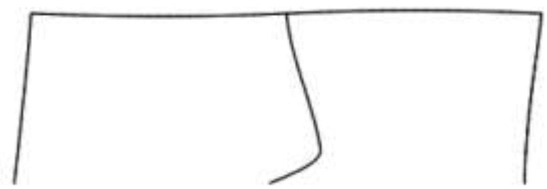

Figure 9 – Buckled shapes of frames in Scenario 7 (worst case delamination in Column 2)

Figure 10 – Buckled shapes of frames in Scenario 13 (worst case delamination in Column 3)

From observing the buckled shapes in Figs. 7 to 10, it can be observed that a configuration similar to symmetric buckling exists in the beams. In fact, 27 of the 32 calibrated values of v_{FN} obtained from the 16 scenarios (one for each beam) were negative. As such, v_{FN} = -1 may have been a more appropriate assumption in producing the un-calibrated results, although the resulting failure times only differ by 3.6% even with assuming v_{FN} = 1. As such, the effect of v_{FN} on the results of the failure time are not very significant in this example. Also, the column with the highest P/P_u ratio in Table 2 appears to experience the most curvature in the buckled shape for each scenario, and the curvature becomes more severe as the corresponding P/P_u ratio approaches unity. The implications of the P/P_u ratio are further explained in the following paragraph.

In the un-calibrated analysis, the frame has a fire resistance of 138.8 min in the undamaged scenario. From Table 2, it can also be seen that damage to the insulation on the beams (Scenarios 4 through 6 and 10 through 12) has the least effect on the fire resistance of the frame. The fire resistance is affected to a greater extent if delamination of the fire protection occurs at the ends of the beams as opposed to in the middle, since the rotational rigidity of the beam-to-column connections is reduced more quickly in these cases. Nevertheless, this reduction is not very significant (up to 5.9% reduction for Scenario 12). Note that in the table, values of $P_i/P_{u,i}$ greater than 0.9 indicate that individual column buckling is imminent, and that the lateral stiffness of the frame is decreasing very quickly at the time of failure. However, it is noted that individual column buckling cannot theoretically occur for non-lean-on columns as the lateral stiffness of the individual column approaches negative infinity as P approaches P_u. As such, the frame will always buckle globally prior to the achievement of individual buckling load. Such is the case when the insulation on any part of Column 2 is damaged (Scenarios 7 through 9), resulting in failure as quickly as 101.4 min. The damage to the insulation on the lower end of Column 2 (Scenario 7) is the worst scenario and represents a 26.9% decrease to the fire resistance of the frame when compared with the undamaged case. It is also worth noting that damage to the insulation near the fixed support (Scenario 13) also significantly reduces the fire resistance of the frame to just 107.6 min (a 22.5% reduction). Overall, the results indicate that insulation damage to Column 2 has the greatest reduction to the failure time of the frame, and it is clear that the effect of blast damage to insulation can significantly reduce the fire resistance of a frame. From a design standpoint, the results of the scenario analysis can be used to identify the most vulnerable locations of a frame and increase the fire resistance in these locations by either strengthening the members or providing more insulation.

5. CONCLUSION

Presented in this paper is a new method for computing the lateral stiffness of an unbraced semi-rigid steel storey frame with three-segmented members, where the three segments in each member can be set to have different input temperatures, or manually prescribed elastic modulus.

The resulting lateral stiffness of the unbraced frame can then be computed. When the lateral stiffness reaches zero, the frame becomes unstable. The proposed methodology can be applied towards many modelling problems where non-linear or piece-wise temperature gradients occur longitudinally in members. A numerical example is presented in which the effects of blast damage to insulation during an ASTM E119 fire event are modelled via a member segment containing delaminated insulation. The proposed method was also validated via finite element analysis as it produces results that are virtually exact to the eigenvalue buckling analysis approach when the value of v_{NF} corresponding to the buckling mode is calibrated. Based on the results of the numerical example, the location of the blast explosion can significantly influence the fire resistance of a frame. The failure mode of the frame can also be changed between individual column buckling depending on the location of fire or blast damage, which reinforces the importance of considering different fire scenarios when analyzing structures.

ACKNOWLEDGEMENTS

The authors wish to thank the National Science and Engineering Research Council (NSERC) [grant number RGPIN-203154-2013] of Canada for the financial support of this work.

REFERENCES

1. Toh WS, Fung TC, Tan KH. Fire resistance of steel frames using classical and numerical methods. J Strc Engr 2000; 127(7):829-838.
2. Couto C, Real PV, Lopes N, Rodrigues P. Buckling analysis of braced and unbraced steel frames exposed to fire. Engr Strc 2013; 49:541-559.
3. Xu L, Zhuang Y. Storey stability of unbraced steel frames subjected to non-uniform elevated temperature distribution. Engr Strc 2014; 62-63:164-173.

4. Rackauskaite E, Kotsovinos P, Rein G. Structural response of a steel-frame building to horizontal and vertical travelling fires in multiple floors. Fire Safety J 2017; 91:542-552.

5. Dwaikat MMS, Kodur VKR. A simplified approach for predicting temperatures in fire exposed steel members. Fire Safety J 2013; 55:87-96.

6. Xu L, Ma T, Zhuang Y. Storey-based stability of unbraced structural steel frames subjected to variable fire loading. J Constr Steel Res 2018; 147:145-153.

7. Ziemian R. Guide to Stability Design Criteria for Metal Structures. 6th ed. Wiley & Sons Ltd; 2010.

8. Yura J. The effective length of columns in unbraced frames. Engr J 1971; 8(2):37-42.

9. LeMessurier W. A practical method of second order analysis Part 2 – Rigid Frames. Engr J 1977; 14(2):49-67.

10. Lui EM. A novel approach for K factor determination. Engr J 1992; 29:150-159.

11. Aristizabal-Ochoa JD. Storey stability of braced, partially braced, and unbraced frames: classical approach. J Str Engr 1997; 123(6):799-807.

12. Xu L. The buckling loads of unbraced PR frames under non-proportional loading. J Constr Steel Res 2001; 58:443-465.

13. Tomecek DV, Milke JA. A study on the effect of partial loss of fire protection on the fire resistance of steel columns. Fire Tech 1993; 29(1): 3-21.

14. Arablouei A, Kodur VKR. Effect of fire insulation delamination on structural performance of steel structures during fire following an earthquake or an explosion. Fire Safety J 2016; 84:40-49.

15. Braxtan NL, Pessiki SP. Postearthquake fire performance of sprayed fire-resistive material on steel moment frames. J Str Engr 2011: 137(9): 946-953.

16. Wang WY, Li GQ, Kodur V. (2013). Approach for modeling fire insulation damage in steel columns. J Strc Engr, 139(4): 491-503.

17. Pettersson O, Magnusson S, Thor J. Fire engineering design of steel structures. Lund, Sweden: Lund Institute of Technology; 1976.

18. Wickström U. Temperature calculation of insulated steel columns exposed to natural fire. Fire Safety J 1981-1982; 4(4):219-225.

19. BSI. BS EN 1993-1.2: 2005 Eurocode 3, Design of steel structures, Part 1.2: General rules – Structural fire design. London, UK: British Standards Institution; 2005.

20. Monforton G, Wu T. Matrix analysis of semi-rigidly connected frames. J Strc Div 1963; 89(6):13-42.

21. Chen KMG. Analysis of Semi-Rigid Connections Subjected to Fire Loads in a Steel Framework (MASc thesis), Waterloo, ON: University of Waterloo; 2010.

22. Al-Jabri KS, Burgess IW, Lennon T, Plank RJ. Moment-rotation-temperature curves for semi-rigid joints. J Constr Steel Res 2005; 61: 281-303.

23. Ramberg W, Osgood WR. Description of stress-strain curves by 3 parameters. National Advisory Committee for Aeronautics; 1943.

24. Xu L, Liu Y. Storey-based effective length factors for unbraced PR frames. Engr J 2002; 39(1):13-29.

25. Liu Y, Xu L. Storey-based stability analysis of multi-storey unbraced frames. Strc Engr Mech 2005; 19(6):679-705.

26. ASTM. Standard Test Methods for fire tests of building construction and materials (ASTM E119-16a). West Conshohocken, PA: American Society for Testing and Materials; 2016.

27. Lie TT. Structural Fire Protection. New York: American Society of Civil Engineers; 1992.

28. Hoblit FM. Buckling load of a stepped column. J Aeronautical Sci 1951; 18(2):124-126.

29. Ypma TJ. Historical development of the Newton-Raphson method. SIAM Review 1995, 37(4):531-551.

30. Zhuang Y. Storey-based Stability Analysis of Unbraced Steel Frames at Ambient and Elevated Temperatures (PhD thesis), Waterloo, ON: University of Waterloo; 2013.

Appendix A Thermal Restraints

For fully restrained columns, the additional axial force H_i may be calculated via Eqs. (A.1). Eqs. (A.1) extend a similar derivation for two-segmented beams in Xu and Zhuang [3] to consider three segments, and the tangent modulus theory from the Eurocode 3 [19] is also applied. In utilizing Eq. (A.1) it is assumed that the differences in axial deformations among columns in the same storey of the frame are ignored [3].

$$H_i = P_i - G_i \tag{A.1a}$$

$$P_i = \frac{G_i + k_i(\Psi_T + \Psi_M(P_i))}{1 + \dfrac{k_i L_{c,i}}{A_{c,i} E_0}} \tag{A.1b}$$

$$\Psi_T = L_{l,i} \int_{T_0}^{T_{l,i}} \alpha(T)dT + L_{m,i} \int_{T_0}^{T_{m,i}} \alpha(T)dT + L_{u,i} \int_{T_0}^{T_{u,i}} \alpha(T)dT \tag{A.1c}$$

$$\Psi_M(P_i) = L_{l,i}\varepsilon_{M,l,i}(P_i) + L_{m,i}\varepsilon_{M,m,i}(P_i) + L_{u,i}\varepsilon_{M,u,i}(P_i) \tag{A.1d}$$

Where $A_{c,i}$ is the cross-sectional area of column i and $\varepsilon_M(P_i)$ is the mechanical strain in the segment as obtained from the Eurocode 3 stress-strain curve in Eq. (A.2) [19]. The terms Ψ_T and Ψ_M refer to the thermal and mechanical deformations, respectively.

$$\varepsilon_M(P) = \begin{cases} {P}/{A_c E} & ; P/A_c \le f_{p,T} \\ \varepsilon_{y,T} - (a/b)\sqrt{b^2 - \left(P/A_c + c - f_{p,T}\right)^2} & ; f_{p,T} < P/A_c < f_{t,Y} \\ \infty & ; P/A_c \ge f_{t,Y} \end{cases} \tag{A.2}$$

Where a, b, and c are the parameters defined in Eurocode 3 [19], and $f_{p,T}$ and $f_{y,T}$ are the proportional limit and yield stress tabulated in Eurocode 3 [19]. As the material may not always be linearly elastic, solving Eq. (A.1a) requires an iteration procedure of computing P_i and converges readily if it is assumed that $P_i = G_i$ on the right-hand side of Eq. (A.1a) in the first iteration. In the numerical example, H_i converges to within only 1.0 N within only four iterations.

α is the coefficient of thermal expansion given in Eq. (A.3) [3] and T_0 is the ambient temperature and may be taken as 20°C.

$$\alpha(T) = (0.004T + 12) \times 10^{-6}\ °\mathrm{C}^{-1} \tag{A.3}$$

k_i is the spring stiffness of the column restraint against axial strains, which may be taken as the total lateral stiffness of the connecting beams. The lateral stiffness of a connecting beam with index j is shown in Eq. (A.4), and is the same as the lateral stiffness of a column rotated on its side, without imperfections or axial loads.

$$k_{i,j} = \frac{12E_0 I_b}{{L_b}^3}\left(\frac{\eta_2 \mu_N \mu_M \mu_F}{12\eta_0 - 2\lambda_{NF}\eta_1 + 6\eta_3 - 9r_N r_F \eta_4}\right) \tag{A.4}$$

Where the subscripts N, M and F correspond to the near, middle and far segments of the beam and the coefficients η_0 through η_4 are given in Eqs. (A.5).

$$\eta_0 = \tau_N \tau_F (1 - r_N)(1 - r_F)\mu_N \mu_M \mu_F \tag{A.5a}$$

$$\eta_1 = 3r_F (1 - r_N)\tau_N + 3r_N (1 - r_F)\tau_F \tag{A.5b}$$

$$\eta_2 = \eta_1 + \frac{9r_N r_F}{L_b}\left(\frac{L_N}{\mu_N} + \frac{L_M}{\mu_M} + \frac{L_F}{\mu_F}\right) \tag{A.5c}$$

$$\eta_3 = 3r_N r_F \lambda_0 + 3r_F (1 - r_N)\tau_N \lambda_F + 3r_N (1 - r_F)\tau_F \lambda_N \tag{A.5d}$$

$$\begin{aligned}\eta_4 = \frac{1}{L_b^4}\Bigg[& L_N^3 (2L_b - L_N)\frac{\mu_M \mu_F}{\mu_N} + L_M^3 (2L_b - L_M)\frac{\mu_N \mu_F}{\mu_M} + L_F^3 (2L_b - L_F)\frac{\mu_N \mu_M}{\mu_F} + \ldots \\ & 2({L_N L_M}^3 \mu_F + {L_N L_F}^3 \mu_M + {L_M L_N}^3 \mu_F + {L_M L_F}^3 \mu_N + {L_F L_N}^3 \mu_M + {L_F L_M}^3 \mu_N) + \ldots \\ & 6({L_N}^2 {L_M}^2 \mu_F + {L_N}^2 {L_F}^2 \mu_M + {L_M}^2 {L_F}^2 \mu_N) + \ldots \\ & 6({L_N}^2 L_M L_F (\mu_M + \mu_F) + {L_M}^2 L_N L_F (\mu_N + \mu_F) + {L_F}^2 L_N L_F (\mu_N + \mu_M)\Bigg]\end{aligned} \tag{A.5e}$$

Where the λ coefficients are given in Eqs. (A.6).

$$\begin{aligned}\lambda_0 = \frac{1}{L_b^3}\Bigg[& L_N^3 \frac{\mu_M \mu_F}{\mu_N} + L_M^3 \frac{\mu_N \mu_F}{\mu_M} + L_F^3 \frac{\mu_N \mu_M}{\mu_F} + 6(L_N L_M L_F \mu_M) + \ldots \\ & 3({L_N}^2 L_M \mu_F + {L_N}^2 L_F \mu_M + {L_M}^2 L_N \mu_F + {L_M}^2 L_F \mu_N + {L_F}^2 L_N \mu_M + {L_F}^2 L_M \mu_N)\Bigg]\end{aligned} \tag{A.6a}$$

$$\lambda_N = \frac{1}{L_b^2}\left[L_N^2\mu_M\mu_F + L_M^2\mu_N\mu_F + L_F^2\mu_N\mu_M + 2(L_N L_M\mu_M\mu_F + L_N L_F\mu_M\mu_F + L_M L_F\mu_N\mu_F)\right] \tag{A.6b}$$

$$\lambda_F = \frac{1}{L_b^2}\left[L_N^2\mu_M\mu_F + L_M^2\mu_N\mu_F + L_F^2\mu_N\mu_M + 2(L_N L_M\mu_N\mu_F + L_N L_F\mu_N\mu_M + L_M L_F\mu_N\mu_M)\right] \tag{A.6c}$$

$$\begin{aligned}\lambda_{NF} = \frac{1}{L_b{}^3}\Big(&L_N^3\mu_M\mu_F + L_M^3\mu_N\mu_F + L_F^3\mu_N\mu_M + \ldots\\ &3L_N L_M^2\mu_N\mu_F + 3L_N L_F^2\mu_N\mu_M + 3L_M L_N^2\mu_M\mu_F + \ldots\\ &3L_F L_M^2\mu_N\mu_F + 3L_F L_N^2\mu_F\mu_M + 3L_M L_F^2\mu_N\mu_M + \ldots\\ &6L_N L_M L_F\mu_N\mu_F\Big)\end{aligned} \tag{A.6d}$$

Note that since H_i is a function of the elastic modulus, which can be a function of the axial load, an iterative solution is required to determine the axial load of the column. However, since H_i is relatively small compared to G_i, the elastic modulus may be taken as a function of just the gravity load rather than the total axial load without introducing significant errors. Doing this prevents the need for an iterative solution, and simplifies the procedure of the time stability assessment.

Appendix B Rotational Buckling

The rotational buckling load of a column, $P_{b,i}$, can be determined by solving for the buckling condition implicitly using the approach outlined by Hoblit [28]. Consider the buckled shape of column i in Fig. B.1. Once again, the subscript i is removed from Fig. B.1 and subsequent equations referring to the variables and properties of this individual column.

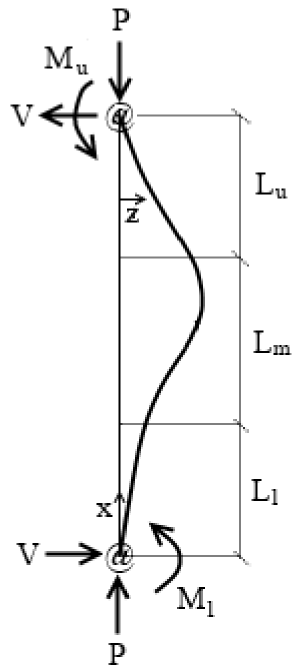

Figure B.1 – Buckled Geometry of a Three-Segment Column

The internal moment in each of the three sections of the column are given in Eqs. (B.1).

$$E_l I_c \frac{d^2 z}{dx^2} = -P_b z(x) + M_l + Vx; \quad 0 \le x \le L_l \tag{B.1a}$$

$$E_m I_c \frac{d^2 z}{dx^2} = -P_b (z(x) - z(L_l)) + M(L_l) + Vx; \quad L_l \le x \le L_l + L_m \tag{B.1b}$$

$$E_u I_c \frac{d^2 z}{dx^2} = -P_b (z(x) - z(L_l + L_m)) + M(L_l + L_m) + Vx; \quad L_l + L_m \le x \le L_c \tag{B.1c}$$

By solving the differential equations in Eqs. (B.1), the bending moment, angle and deflection of the column can be obtained at the upper and lower ends of the column, as well as the points between adjacent segments. Thus, for buckling to occur, Eqs. (B.2) must be satisfied.

$$z(0)=0 \tag{B.2a}$$

$$z(L_l)=z(0)+\frac{M(0)}{P_b}-\frac{M(0)}{P_b}C_l+\frac{z'(0)-V/P_b}{\phi_l/L_c}S_l+\frac{VL_l}{P_b} \tag{B.2b}$$

$$z(L_l+L_m)=z(L_l)+\frac{M(L_l)}{P_b}-\frac{M(L_l)}{P_b}C_m+\frac{z'(L_l)-V/P_b}{\phi_m/L_c}S_m+\frac{VL_m}{P_b} \tag{B.2c}$$

$$z(L_c)=z(L_l+L_m)+\frac{M(L_l+L_m)}{P_b}-\frac{M(L_l+L_m)}{P_b}C_u+\frac{z'(L_l+L_m)-V/P_b}{\phi_u/L_c}S_u+\frac{VL_u}{P_b} \tag{B.2d}$$

$$z(L_c)=0 \tag{B.2e}$$

$$z'(L_l)=\frac{M(0)}{P_b}\left(\frac{\phi_l}{L}\right)S_l+\left(z'(0)-V/P_b\right)C_l+\frac{V}{P_b} \tag{B.2f}$$

$$z'(L_l+L_m)=\frac{M(L_l)}{P_b}\left(\frac{\phi_m}{L}\right)S_m+\left(z'(L_l)-V/P_b\right)C_m+\frac{V}{P_b} \tag{B.2g}$$

$$z'(L_c)=\frac{M(L_l+L_m)}{P_b}\left(\frac{\phi_u}{L}\right)S_u+\left(z'(L_l+L_m)-V/P_b\right)C_u+\frac{V}{P_b} \tag{B.2h}$$

$$M(0)=+R_l z'(0) \tag{B.2i}$$

$$M(L_l)=M(0)C_l-\left(z'(0)-V/P_b\right)\frac{P_bL_c}{\phi_l}S_l \tag{B.2j}$$

$$M(L_l+L_m)=M(L_l)C_m-\left(z'(L_l)-V/P_b\right)\frac{P_bL_c}{\phi_m}S_m \tag{B.2k}$$

$$M(L_c)=M(L_l+L_m)C_u-\left(z'(L_l+L_m)-V/P_b\right)\frac{P_bL_c}{\phi_u}S_u \tag{B.2l}$$

$$M(L_c)=-R_l z'(L_c) \tag{B.2m}$$

$$V_i=\frac{-z'(0)(R_l\beta_1+L_cP_b\beta_2)}{L_c\beta_3} \tag{B.2n}$$

Where the coefficients β_1, β_2 and β_3 are given in Eqs. (23).

$$\beta_1=\phi_l\phi_m\phi_u(1-C_lC_mC_u)+\phi_l^2\phi_uS_lS_mC_u+\phi_l^2\phi_mS_lC_mS_u+\phi_l\phi_m^2C_lS_mS_u \tag{B.3a}$$

$$\beta_2=\phi_l\phi_mC_lC_mS_u+\phi_l\phi_uC_lS_mC_u+\phi_m\phi_uS_lC_mC_u-\phi_m^2S_lS_mS_u \tag{B.3b}$$

$$\beta_3=\phi_l\phi_m\phi_u+\phi_m^2S_lS_mS_u-\phi_l\phi_mC_lC_mS_u-\phi_l\phi_uC_lS_mC_u-\phi_m\phi_uS_lC_mC_u \tag{B.3c}$$

Where ϕ_l, ϕ_m, ϕ_u, S_l, S_m, S_u, C_l, C_m and C_u are all shown in Eqs. (16). The lowest value of P_b that satisfies Eqs. (B.2) may be taken as the final value $P_{b,i}$ for column i. The minimum value of P_b satisfying the system of fourteen equations in Eqs. (B.2) can be obtained by using root-finding algorithms, such as the Newton-Raphson method [29].

Appendix C End Fixity Factors for Three-Segment Members

The end fixity factor for two-segmented members was previously derived by Zhuang [30]. A new, similar derivation is presented in following for the end fixity factors of three-segment members. Note that the derivation applies for both beams and columns. The end fixity factor is defined as the ratio between the rotation at the end of the member, α, and the combined rotation, ϕ, of the member and connection due to a unit end-moment, as shown in Fig. C.1.

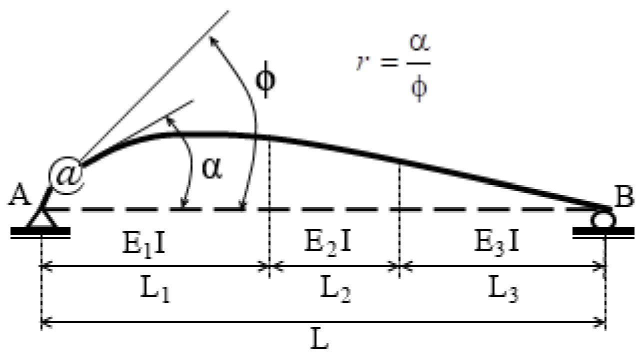

Figure C.1 – Definition of end fixity factor for a three-segmented member

Based on this relation, Zhuang [30] showed that the end fixity factor can be derived by determining the end rotation of an equivalent simply-supported member, R_{SS}, subjected to a unit end moment at the same end and substituting the result into Eq. (C.1).

$$r = \frac{\alpha}{\phi} = \frac{R}{R + R_{SS}} \tag{C.1}$$

Where R is the rotational rigidity of the semi-rigid connection. For a member with uniform cross-section, R_{SS} may be taken as $3EI/L^3$, which results in the end fixity factors derived in [20]. Zhuang [30] showed that R_{SS} for a two-segment member can be derived using the principle of virtual work. Using the same methodology, the principle of virtual work is henceforth applied towards three-segment members. Consider the simply supported member in Fig. C.2.

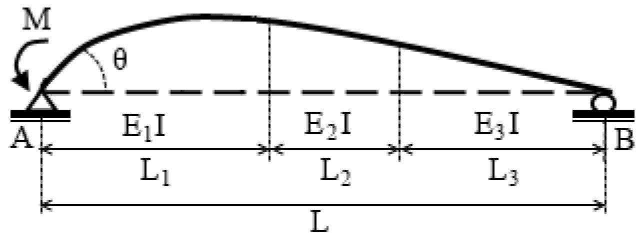

Figure C.2 – Equivalent simply-supported three-segment member subjected to unit end moment

The virtual work principle is applied at the location of the end moment, *M*, on end *A* of the member in Eq. (C.2).

$$1\times\theta=\int_{0}^{L_1}\frac{Mx^2}{L^2E_1I}\,dx+\int_{L_1}^{L_1+L_2}\frac{Mx^2}{L^2E_2I}\,dx+\int_{L_1+L_2}^{L}\frac{Mx^2}{L^2E_3I}\,dx \qquad \text{(C.2)}$$

The value of the end rotation θ at *A* is therefore obtained via integration in Eq. (C.2). The value of R_{SS} can then be obtained by dividing the moment *M* by θ and substituting the elastic modulus degradation factors from Eq. (1) to obtain Eq. (C.3).

$$R_{SS}=\frac{M}{\theta}=\frac{3E_0I}{L}\left(\frac{1}{\tau}\right) \qquad \text{(C.3)}$$

Where τ is an adjustment factor that accounts for the non-uniformity of the elastic modulus in the member, and is expressed in Eqs. (4) based on end moments being applied on the corresponding ends of the members. Thus, substituting Eq. (C.3) into Eq. (C.1) yields the end fixity factor equation in Eqs. (3).

Appendix D Equivalent Rotational Stiffness of Connecting Beams

The rotational rigidity of a beam being connected to the end of a column is derived in this appendix by utilizing the slope-deflection and conjugate-beam methods, similar to the approach demonstrated in [20] but extended for three-segmented members. Consider first the deformation of the beam shown in Fig. D.1.

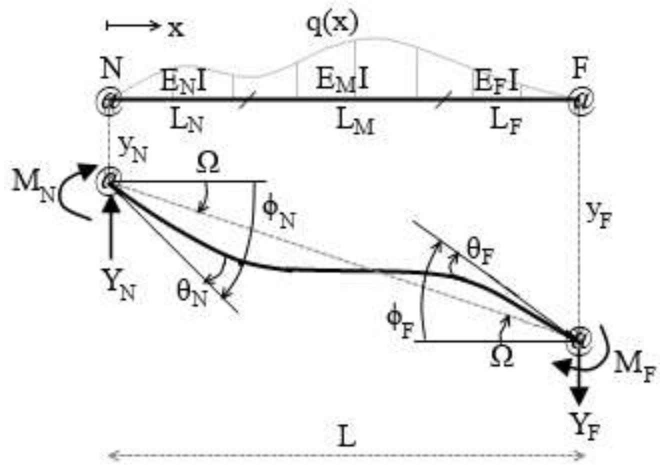

Figure D.1 – Generalized three-segment beam subjected to end moments

The near and far ends of the beam in Fig. D.1 are denoted as *N* and *F*, respectively. The subscript *M* denotes the middle segment of the beam. The displacement symbols y, ϕ, θ and Ω correspond to the end deflection, rotation of the connection, net rotation between the member end and connection, and chord rotation, respectively. The force symbols *Y*, *q* and *M* correspond to the transverse reaction, transverse load function and end moments, respectively. Then the internal moment can be expressed in Eq. D.1.

$$M(x) = \int_0^x \int_0^x q(x) dx^2 + C_1 x + C_2 \tag{D.1}$$

Where C_1 and C_2 are integration constants. The boundary conditions for Eq. (D.1) are given in Eqs. (D.2).

$$M(0) = M_N \tag{D.2a}$$

$$M(L) = -M_F \tag{D.2b}$$

Substituting the boundary conditions into Eq. (D.1) to solve for the constants results in the internal moment equation in Eq. (D.3).

$$M(x) = \int_0^x \int_0^x q(x)dx^2 + M_N\left(1 - \frac{x}{L}\right) + M_F\left(\frac{x}{L}\right) - \frac{x}{L}\int_0^L \int_0^L q(x)dx^2 \tag{D.3}$$

Traditionally in stability analysis, loads are assumed to be directly applied to the columns and the only effect of the connected beam being considered is the rotational restraint [12]. As such, it is assumed that no transverse loads are applied on the beam between the ends ($q(x) = 0$). Then let $c(x)$ be obtained by dividing $M(x)$ by $E(x)I$, resulting in Eq. (D.4).

$$c(x) = \frac{M_N}{E(x)I}\left(1 - \frac{x}{L}\right) + \frac{M_F}{E(x)I}\left(\frac{x}{L}\right) \tag{D.4}$$

Due to the piece-wise nature of $E(x)$ in the three-segment beam, $c(x)$ is piece-wise and can be split into individual functions of the local coordinates in each segment. Let the local coordinates x_N, x_M and x_F correspond to the near, middle and far segments, given in Eqs. (D.5).

$$x_N = x; \quad 0 \le x_N \le L_N \tag{D.5a}$$
$$x_M = x - L_N; \quad 0 \le x_M \le L_M \tag{D.5b}$$
$$x_F = x - (L_N + L_M); \quad 0 \le x_F \le L_F \tag{D.5c}$$

Then the corresponding local functions c are given in Eqs. (D.6).

$$c_N(x_N) = \frac{M_N}{\mu_N E_0 I}\left(1 - \frac{x_N}{L}\right) - \frac{M_F}{\mu_N E_0 I}\left(\frac{x_N}{L}\right) \tag{D.6a}$$
$$c_M(x_M) = \frac{M_N}{\mu_M E_0 I}\left(1 - \frac{L_N}{L} - \frac{x_M}{L}\right) - \frac{M_F}{\mu_M E_0 I}\left(\frac{L_N}{L} + \frac{x_M}{L}\right) \tag{D.6b}$$
$$c_F(x_F) = \frac{M_N}{\mu_F E_0 I}\left(1 - \frac{L_N}{L} - \frac{L_M}{L} - \frac{x_F}{L}\right) - \frac{M_F}{\mu_F E_0 I}\left(\frac{L_N}{L} + \frac{L_M}{L} + \frac{x_F}{L}\right) \tag{D.6c}$$

Let A_N, A_M and A_F be the areas under the curves c_N, c_M and c_F over their corresponding domains, respectively, expressed in Eq. (D.7).

$$A_N = \int_0^{L_N} c_N(x_N)dx_N \tag{D.7a}$$

$$A_M = \int_0^{L_M} c_M(x_M)\,dx_M \tag{D.7b}$$

$$A_N = \int_0^{L_N} c_N(x_N)\,dx_N \tag{D.7c}$$

The total area under *c(x)* is therefore $A = A_N + A_M + A_F$, and the centroid, $\bar{x}$, of *c(x)* can be expressed in Eq. (D.8).

$$\bar{x} = \frac{\bar{x}_N A_N + \bar{x}_M A_M + \bar{x}_F A_F}{A} \tag{D.8}$$

Where $\bar{x}_N$, $\bar{x}_M$ and $\bar{x}_F$ are the global *x* coordinates of the centroids in each of the functions c_N, c_M and c_F, respectively, and given in Eqs. (D.9).

$$\bar{x}_N A_N = \int_0^{L_N} x_N c_N(x_N)\,dx_N \tag{D.9a}$$

$$\bar{x}_M A_M = \int_0^{L_M} (x_M + L_N) c_M(x_M)\,dx_M \tag{D.9b}$$

$$\bar{x}_F A_F = \int_0^{L_F} (x_F + L_N + L_M) c_F(x_F)\,dx_F \tag{D.9c}$$

By the conjugate beam method, the rotations of the beam ends are related to *c* by Eqs. (D.10).

$$\theta_N - \phi_N - \Omega = A\left(1 - \frac{\bar{x}}{L}\right) \tag{D.10a}$$

$$\theta_F - \phi_F - \Omega = -A\left(\frac{\bar{x}}{L}\right) \tag{D.10b}$$

Assume that $\Omega = 0$, since the columns in the frame are not expected to experience significant differential axial deformations. Also, since the ends of the beam are semi-rigidly connected, ϕ can be expressed in terms of the end moments and rotational rigidities according to Eq. (D.11).

$$\phi_N = M_N / R_N \tag{D.11a}$$

$$\phi_F = M_F / R_F \tag{D.11b}$$

Where *R* can be obtained by rearranging Eqs. (3). Thus, substituting Eqs. (D.11) into Eqs. (D.10) and solving explicitly for M_N yields the end moments given in Eqs. (D.12).

$$M_N = \frac{6E_0 I r_N}{L}\left[\frac{2\tau_F \mu_L \mu_M \mu_R (1-r_F)\theta_N + 2\lambda_{NN} r_F \theta_N + \lambda_{NF} r_F \theta_F}{4\lambda_A + r_N \lambda_B + r_F \lambda_C - r_N r_F \lambda_D}\right] \tag{D.12}$$

Note that swapping the coefficients N and F in the terms of Eq. (12) yields M_F. Finally, the beam rotational stiffness contribution to the end of the connected column, $R_{i,j}$ in Eq. (6), is obtained by dividing Eq. (D.12) by θ_N.